

Numerical studies of the nonlinear properties of composites

X. Zhang and D. Stroud

Department of Physics, Ohio State University, Columbus, Ohio 43210

(Received 29 June 1993; revised manuscript received 29 November 1993)

Using both numerical and analytical techniques, we investigate various ways to enhance the cubic nonlinear susceptibility χ_e of a composite material. We start from the exact relation $\chi_e = \sum_i p_i \chi_i \langle (\mathbf{E} \cdot \mathbf{E})^2 \rangle_{i,\text{lin}} / E_0^4$, where χ_i and p_i are the cubic nonlinear susceptibility and volume fraction of the i th component, E_0 is the applied electric field, and $\langle E^4 \rangle_{i,\text{lin}}$ is the expectation value of the electric field in the i th component, calculated in the linear limit where $\chi_i = 0$. In our numerical work, we represent the composite by a random resistor or impedance network, calculating the electric-field distributions by a generalized transfer-matrix algorithm. Under certain conditions, we find that χ_e is greatly enhanced near the percolation threshold. We also find a large enhancement for a linear fractal in a nonlinear host. In a random Drude metal-insulator composite χ_e is hugely enhanced especially near frequencies which correspond to the surface-plasmon resonance spectrum of the composite. At zero frequency, the random composite results are reasonably well described by a nonlinear effective-medium approximation. The finite-frequency enhancement shows very strong reproducible structure which is nearly undetectable in the linear response of the composite, and which may possibly be described by a generalized nonlinear effective-medium approximation. The fractal results agree qualitatively with a nonlinear differential effective-medium approximation. Finally, we consider a suspension of coated spheres embedded in a host. If the coating is nonlinear, we show that $\chi_e / \chi_{\text{coat}} \gg 1$ near the surface-plasmon resonance frequency of the core particle.

I. INTRODUCTION

The electrical and optical properties of composite media can differ dramatically from those of their constituents.^{1,2} In a simple picture, these differences arise from local electric-field fluctuations. The constitutive properties (i.e., the conductivity or the dielectric function) vary widely within the composite. This leads to similar variation in the local electric fields and currents and, hence, to large enhancements or decreases in averaged quantities, relative to their values in homogeneous media.

In this paper, we are concerned with the cubic nonlinear properties of various binary composites. Nonlinearities in composites have attracted considerable recent attention, both at zero frequency³⁻¹³ and at finite frequencies.¹⁴⁻¹⁹ In materials with cubic nonlinearities, the electric displacement \mathbf{D} and electric field \mathbf{E} are related by

$$\mathbf{D} = \epsilon \mathbf{E} + \chi |\mathbf{E}|^2 \mathbf{E}, \quad (1)$$

where ϵ and χ are the (position-dependent) dielectric function and cubic nonlinear susceptibility. As has been discussed elsewhere,⁹ the *effective* composite susceptibility χ_e can be enormously enhanced, relative to its value in a homogeneous medium. As in linear media, this enhancement arises from local field fluctuations, which play an even larger role in nonlinear than in linear response functions.¹²

Enhanced nonlinear response is of both fundamental and practical interest. Like the linear response functions, the nonlinear ones diverge near a percolation threshold. The analytic form of this divergence is of interest as a

critical phenomenon. From a practical viewpoint, materials with large χ_e 's may be useful as optical elements, e.g., as fast intensity-dependent optical filters.¹⁴

In this paper, we consider a variety of ways to enhance the χ_e 's of composite media. In many calculations, we model these composites as random impedance or resistance networks. While obviously idealized as descriptions of real materials, these models can be accurately treated numerically. Using recently developed approaches, not only the effective impedances of the networks,²⁴ but also the *distribution* of electric fields or displacements²⁵ can be calculated. The fourth moments of these distributions are related, by an exact theorem,⁹ to χ_e of the networks.

We also compare our numerical result to simple approximations. For random composites at zero frequency, a nonlinear effective-medium approximation¹⁰ qualitatively describes our results. When one of the components is distributed in a nonrandom fashion, e.g., fractally, the numerical results appear consistent with a differential effective-medium approximation which is an extension of a previous linear approach.²⁰ This approach correctly predicts a large enhancement of χ_e when linear fractals are embedded in a nonlinear host. Our numerical results for random networks at finite frequencies may be consistent with a somewhat generalized effective-medium approximation. More important, χ_e for such networks exhibits a great deal of structure in frequency which is nearly undetectable in the underlying linear response.

Besides network models, we also consider a distribution of small spheres of linear material with a nonlinear coating and embedded in a linear host. The nonlinear response of the coating is hugely increased at certain

characteristic frequencies close to the surface-plasmon resonance of the underlying sphere. We present simple model calculations of this enhancement, assuming Au core particles, and using the fourth moment formalism of Ref. 9. Our results are analogous to that predicted for a metallic coating on a nonlinear spheroidal particle, using a somewhat different approach,²¹ and are formally similar to those of Ref. 22.

We turn now to the body of the paper. Section II reviews the formal basis of our calculations and our method of calculation. Section III gives numerical results for random composites at zero frequency, and compares these with a nonlinear effective-medium approximation. Numerical results for fractal clusters in two dimensions ($d=2$) are presented in Sec. IV, and compared to the predictions of a nonlinear differential effective-medium approximation. Random media at finite frequencies are treated in Sec. V. Numerical results for coated spheres are given in Sec. VI, followed by a brief discussion in Sec. VII.

II. FORMALISM AND METHOD

The basis of our method is an exact result proved by several authors,^{9,23} which connects χ_e to the fourth moment of the electric field in the *linear* limit. We describe this result first at zero frequencies. Consider a composite in which the local current density $\mathbf{J}(\mathbf{x})$ and electric field $\mathbf{E}(\mathbf{x})$ are related by

$$\mathbf{J}(\mathbf{x}) = \sigma(\mathbf{x})\mathbf{E}(\mathbf{x}) + \chi(\mathbf{x})|\mathbf{E}(\mathbf{x})|^2\mathbf{E}(\mathbf{x}), \quad (2)$$

where $\sigma(\mathbf{x})$ and $\chi(\mathbf{x})$ are the local conductivities and cubic nonlinear susceptibilities. Then the theorem^{9,23} states that the *effective* nonlinear susceptibility χ_e is given by

$$\chi_e = \frac{\sum_i p_i \chi_i \langle (\mathbf{E} \cdot \mathbf{E})^2 \rangle_{i,\text{lin}}}{E_0^4}, \quad (3)$$

where $\langle \dots \rangle_{i,\text{lin}}$ denotes a volume average over the volume of the i th component in the *linear* limit (i.e., when $\chi_i=0$), p_i is the volume fraction of component i , and E_0 is the space-average field within the composite. This theorem is very useful, because it connects the composite nonlinear response to the nonlinear response functions of the constituents, and an average over the *linear* properties of the composite.

To separate these dependences more explicitly we introduce *enhancement factors*

$$e_i = \frac{\langle (\mathbf{E} \cdot \mathbf{E})^2 \rangle_{i,\text{lin}}}{E_0^4}, \quad (4)$$

in terms of which

$$\chi_e = \sum_i p_i \chi_i e_i. \quad (5)$$

Evidently, e_i is the fractional increase of the fourth moment of the electric field in the i th component relative to its applied value. It represents the factor by which the nonlinear susceptibility of the i th component is enhanced, per unit volume, in the composite.

A useful approximation for an average in Eq. (3) is to make the approximate factorization^{10,18}

$$\langle (\mathbf{E} \cdot \mathbf{e})^2 \rangle_{i,\text{lin}} \approx \langle (\mathbf{E} \cdot \mathbf{E}) \rangle_{i,\text{lin}}^2. \quad (6)$$

This factorization is sometimes termed the “nonlinear effective-medium approximation” (EMA) because it approximates the spatially fluctuating electric field within one component by a single value. We expect it to be most accurate when fluctuations in the electric field *within* one component are not too large. Since $\langle (\mathbf{E} \cdot \mathbf{E}) \rangle_{i,\text{lin}}$ is given *exactly* by¹²

$$\frac{p_i \langle E^2 \rangle_i}{E_0^2} = \frac{\partial \sigma_e}{\partial \sigma_i} \equiv F_i, \quad (7)$$

where σ_e and σ_i are, respectively, the effective conductivity of the composite and of the i th component, it follows that χ_i can be written approximately as

$$\chi_e = \sum_i \chi_i F_i^2 / p_i \quad (8)$$

or equivalently $e_i = F_i^2 / p_i^2$.

The EMA is completed by calculating σ_e (or equivalently F_i) from some approximation. One possible approximation for σ_e is, of course, the *linear* effective-medium approximation, which in d dimensions is given by

$$\sum_i p_i \frac{\sigma_i - \sigma_e}{\sigma_i + (d-1)\sigma_e} = 0. \quad (9)$$

However, one may still make the decoupling approximation (6) in conjunction with some other approximation for σ_e .¹⁰ Indeed, we find in the calculations below that the nonlinear EMA works reasonably well at finite frequencies only if the correct form for σ_e (or, at finite frequencies, ϵ_e) is used in Eq. (8).

Equation (3) is readily generalized to finite frequencies, provided one makes the “quasistatic approximation,” where \mathbf{E} is expressed as the negative gradient of an electrostatic potential. This is usually reasonable for inhomogeneities much smaller than the wavelength of light in the medium. In the quasistatic limit, the composite is conveniently described in terms of a displacement field \mathbf{D} , whose imaginary part is related to the usual transport current density,

$$\mathbf{D}(\mathbf{x}) = \epsilon(\mathbf{x})\mathbf{e}(\mathbf{x}) + \chi(\mathbf{x})|\mathbf{E}(\mathbf{x})|^2\mathbf{E}(\mathbf{x}), \quad (10)$$

and χ_e is given by expressions similar to (3) and (5):

$$\chi_e = \frac{\sum_i \chi_i \langle (\mathbf{E} \cdot \mathbf{E}^*)(\mathbf{E} \cdot \mathbf{E}) \rangle_{i,\text{lin}}}{E_0^4} \equiv \sum_i p_i e_i \chi_i. \quad (11)$$

Here $\mathbf{E}(\mathbf{x})$ now denotes a complex quantity, such that the physical electric field at position \mathbf{x} at time t is $\text{Re}[\mathbf{E}(\mathbf{x})\exp(-i\omega t)]$. All quantities in Eqs. (10) and (11) are frequency dependent, and the averages $\langle \dots \rangle_{i,\text{lin}}$ are still to be carried out in the related linear material.

The decoupling approximation (6) can also be generalized to finite frequencies, with the results

$$\chi_e = \sum_i \chi_i F_i |F_i| / p_i, \quad (12)$$

where now

$$F_i = \frac{\partial \epsilon_e}{\partial \epsilon_i}, \quad (13)$$

and ϵ_e and ϵ_i are the complex, frequency-dependent dielectric functions of the effective medium and of the i th component. If one chooses to calculate ϵ_e in the linear EMA, then ϵ_e satisfies

$$\sum_i p_i \frac{\epsilon_i - \epsilon_e}{\epsilon_i + (d-1)\epsilon_e} = 0. \quad (14)$$

In most of our calculations, we will apply Eqs. (3) or (11) to a binary composite modeled as a cubic mesh of impedances in two or three dimensions ($d=2$ or 3). The impedances are of two types, generally denoted A or B , and are distributed according to various random algorithms as described below. The effective *linear* conductances or admittances of the networks are calculated using the transfer-matrix algorithm.²⁴ The distribution of electric fields is obtained using a generalization of this algorithm due to Duering *et al.*²⁵ These distributions are needed to calculate the fourth moments from which χ_e is calculated at either zero or finite frequencies. The networks are assumed to be $L_x \times L_z$ or $L_x \times L_x \times L_z$ in two or three dimensions (with $L_z \gg L_x$ and all the L 's integer). With this choice of sample, we effectively average over (L_z/L_x) realizations of cubic samples of size L_x^d . The boundaries at $x=0$ and $x=L_x$ are held at potentials 0 and V , respectively. In three dimensions, we impose periodic boundary conditions in the y direction (this issue does not arise in two dimensions). Further details of the numerical method are given in Refs. 25 and 30.

III. RANDOM BINARY COMPOSITES IN THREE DIMENSIONS: ZERO FREQUENCY

We begin by considering a $d=3$ network having two types of bonds, A and B , with conductances g_A and g_B ($g_A > g_B$), present in proportions p_A and $p_B \equiv 1-p_A$, and distributed at random in the composite. Our calculation is carried out for $L_x=10$, $L_z=2500$, equivalent to averaging over 250 samples of size 10^3 .

Figures 1(a) and 1(b) show the relative enhancements e_A and e_B , plotted as functions of p_A for $g_A=10^4$, $g_B=1$, and for $g_A=10^3$, $g_B=1$. Clearly, e_B has sharp maxima near the percolation threshold ($p_A=0.2492$) where the A bonds would first form an infinite connected cluster in an infinite sample. The enhancement is about a factor of 100 for $g_A/g_B=10^4$, and somewhat less for $g_A/g_B=10^3$. e_A exhibits no peak near $p_A=0.25$. The large values of e_B near percolation can presumably be understood in terms of large current distortions (and consequent field enhancements) near the tips of the large clusters that form near percolation. The greater enhancement for the larger ratio g_A/g_B can also be understood in this way: The larger this ratio, the more radically the fields are distorted, leading to larger field enhancements.

We now compare these results with the predictions of the nonlinear effective-medium approximation, assuming *both* the decoupling approximation [Eq. (6)] and the linear EMA [Eq. (9)]. Figures 2(a) and 2(b) show the EMA enhancements e_A and e_B corresponding to the examples of Fig. 1. Evidently the EMA predicts, at least qualitatively, the sharp increase in e_B near the percolation threshold. Similar results using a slightly different method, and comparable agreement with the EMA, have been obtained by Yang and Hui²⁶ in $d=2$.

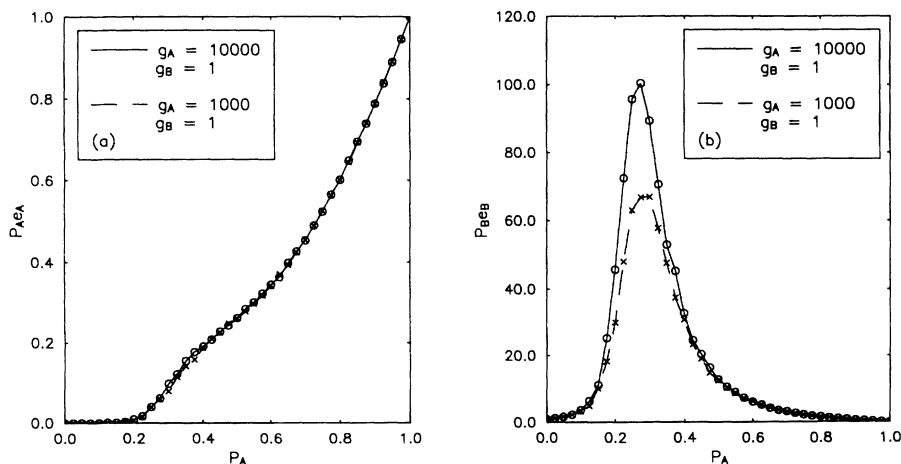


FIG. 1. Enhancement of χ_e in a three-dimensional ($d=3$) random binary composite of two conductors at zero frequency, as calculated numerically. In both (a) and (b), the solid curves correspond to A and B bonds having conductances $g_A=10000$, $g_B=1$, while the dashed curves represent $g_A=1000$, $g_B=1$. In (a) and (b) we plot $p_A e_A$ and $p_B e_B$, where $e_i \equiv \langle E^4 \rangle_i / E_0^4$ and p_i is the concentration of bonds of type i for these two cases. $\langle E^4 \rangle_i$ represents the average of the fourth power of the electric field in a bond of type i ; E_0 is the applied electric field.

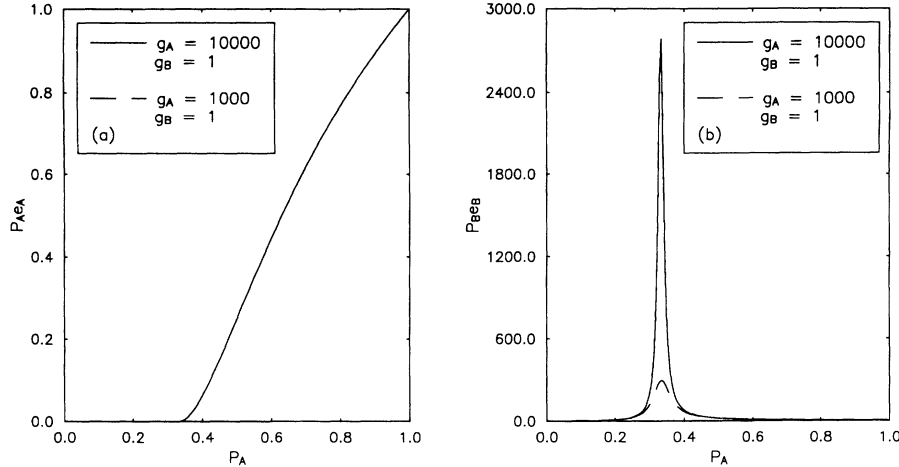


FIG. 2. Same as Fig. 1, but calculated using the effective-medium approximation.

We now try to interpret the critical behavior near p_c^A in the light of previous work on network properties near the percolation threshold. In the limit $g_A/g_B \rightarrow \infty$, it is expected that

$$e_A \propto |p - p_c^A|^{\kappa + 2t}, \quad (15)$$

$$e_B \propto |p - p_c^A|^{-\kappa - 2s}. \quad (16)$$

Here t and s are the usual percolation critical exponents, defined by

$$\sigma_e \propto \sigma_A (p_A - p_c)^t \quad (p > p_c), \quad (17)$$

$$\sigma_e \propto \sigma_B (p_c - p_A)^{-s} \quad (p < p_c), \quad (18)$$

while κ and κ' describe the critical behavior of random resistance fluctuations near p_c^A . Using estimates based on a nodes-links-blobs model of the infinite cluster near p_c , Wright *et al.*¹³ have proposed the bounds $1.53 \leq \kappa \leq 1.60$, $0.38 \leq \kappa' \leq 1.02$. Combined with the currently accepted estimates $t \approx 2.0$ and $s \approx 0.77$ for lattice percolation in $d = 3$, these imply

$$e_A \approx (p - p_c)^{2.4 \pm 0.1} \quad (p > p_c), \quad (19)$$

$$e_B \approx (p_c - p)^{-2.2 \pm 0.4} \quad (p < p_c), \quad (20)$$

where the quoted uncertainties are simply guesses based on the bounds for κ and κ' and the postulated very small error bars on s and t .

Equation (20) implies a strong divergence in e_B in $d = 3$, consistent with both our simulations and the EMA.

It seems somewhat surprising that e_B^{EMA} is actually larger than that obtained numerically. We speculate that this is an artifact of the finite L_x . In the limit of very large g_A/g_B , Eq. (16) implies that $e_B \propto \xi_p^{(\kappa' + 2s)/\nu}$, where ξ_p is the percolation correlation length which diverges on either side of p_c^A according to the power law $\xi_p \propto |p - p_c|^{-\nu}$. Since ξ_p is bounded by the finite transverse dimension L_x , the numerically calculated e_B cannot exceed an upper bound proportional to $L_x^{(k' + 2s)/\nu}$. In our system, where L_x is only 10, this limits the growth of e_B . If we were able to carry out our calculations on samples with larger cross sections, we expect that the peak in

e_B would be larger, and perhaps comparable to the EMA result.

IV. FRACTAL DISTRIBUTIONS IN TWO DIMENSIONS

Since a fractal bond fractal distribution can greatly influence the *linear* response of composites,²⁷ it is plausible that fractals will have similar influence on the *non-linear* response. We now consider this question, restricting ourselves to $d = 2$, in which relatively large fractals can be considered.

As in $d = 3$, we assume two types of bonds, with conductivities g_A and g_B ($g_A > g_B$), present in concentrations p_A and $1 - p_A$. The A bonds are arranged in an ordered "cross" fractal of stage k , and embedded in a matrix of B bonds.²⁷ The fractal is initiated by embedding a cross of four A bonds in a B matrix. A stage- k cross fractal is constructed by adding four stage- $(k - 1)$ fractals to the sides of a central stage- $(k - 1)$ fractal (cf. Fig. 2 of Ref. 27). Thus, a stage- k cluster contains $4 \times 5^{k-1}$ bonds, spans a linear dimension $2 \times 3^{k-1}$, and has fractal dimension $d_f = \ln 5 / \ln 3$.

Table I gives our results for ordered fractals in various-sized lattices, assuming $g_A = 10^4$, $g_B = 1$. For ease of comparison, the network in each case has a linear dimension four bonds larger than the enclosed fractal. Evidently, $e_B \gg 1$, while e_A shows no enhancement. Furthermore, e_B increases strikingly with increasing k . We have also calculated e_A and e_B in fractal networks for which the (fractally arranged) type- B bonds have the larger conductance ($g_A = 10^{-4}$, $g_B = 1.0$). The results (Table II) show that this type of network produces a smaller enhancement than the reverse situation, but that the nonlinear enhancement is still substantial.

For comparison, we also list e_A and e_B in *random* two-dimensional networks in which g_A and g_B have the same values as in the fractal networks. For analogous concentrations of A and B bonds, e_B is orders of magnitude smaller than in the fractal networks.

It may appear surprising that e_B appears to diverge with increasing k in Tables I and II, even though the *fraction* of bonds in the fractal is decreasing towards zero.

TABLE I. Enhancement of nonlinear susceptibility in two-dimensional square networks containing cross fractals (fractal dimension $\ln 5/\ln 3$) at various stages. The linear dimension of a cross fractal at stage k is $2 \times 3^{k-1}$, and it contains $4 \times 5^{(k-1)}$ bonds. The columns denote the fractal stage, the linear dimension of the fractal, the linear dimension of the network, the real fraction of type- A bonds, and the average value of E^4 on an A bond and on a B bond (normalized to the applied electric field). The last row corresponds to a random distribution of A bonds. In all these networks, $g_A = 10^4$, $g_B = 1$.

Stage	Size	NW ^a size	p_A	e_A	e_B
3	18	22	0.103	0.105	22.686
4	54	58	0.0743	0.093	178.83
5	162	166	0.0454	0.064	1383.1
Random	N/A	166	0.100	0.175	1.6447

^aNetwork.

This is probably because the lattice sizes in these tables are always four bonds longer than the enclosed fractal. Thus, although the density of A does indeed go to zero as the stage k goes to infinity, one is still not exactly in the “dilute limit” in which the influence of the fractal is confined to a small fraction of the total area. As one can see from the equipotentials shown in Figs. 3(a) and 3(b) (and discussed further below), the influence of the fractal actually extends over a number of bonds comparable to its *area*, not just the actual number of A bonds. This area is not a small fraction of the lattices considered (in fact, it is a fraction which increases with k). This is why, we believe, the factor e_B seems to diverge as k increases for these lattices.

Our fractal results are generally consistent with expectations based on calculations for random composites. As described in the previous section, such systems have a divergent nonlinear response near the percolation threshold. According to some models, a composite close to the percolation may have a fractal-like structure, with a correlation length ξ_p which grows as percolation is approached. In this sense, a larger fractal is like a system closer to percolation. It should therefore have a larger χ_e than a smaller fractal, as we observe. Furthermore, just as in the random case, the enhancement is larger when the “noncritical” component, i.e., the material outside the fractal, has the lower conductivity.

The reader may be concerned that a suspension of fractal clusters is not exactly analogous to a percolation threshold, because near p_c there are, in addition to the infinite fractal cluster, many finite clusters with a variety

TABLE II. Same as Table I, but $g_A = 10^{-4}$, $g_B = 1$.

Stage	Size	NW size	p_A	e_A	e_B
3	18	22	0.103	0.343	1.229
4	54	58	0.0743	0.814	4.787
5	162	166	0.0454	5.856	138.0

of length scales. This is certainly a valid concern, and, therefore, the connection between the two geometries can only be a loose one. Our point here, however, is only that *numerically* similar behavior seems to be occurring in both types of systems.

As already mentioned, our results for a given stage of fractal depend sensitively on the size of the embedding network. To illustrate this, we have calculated the nonlinear response of three samples generated from the same fractal but with different network sizes, always assuming $g_A = 10^4$, $g_B = 1$ (cf. Table III). Evidently, e_B falls off dramatically with increasing network size. To explain this, we show in Figs. 3(a) and 3(b) the electrostatic potential for a stage-4 fractal embedded in a 58×58 network and a 100×100 network. Obviously, the electric-field enhancement near the fractal tip is enormous when the fractal nearly spans the sample, while for the larger

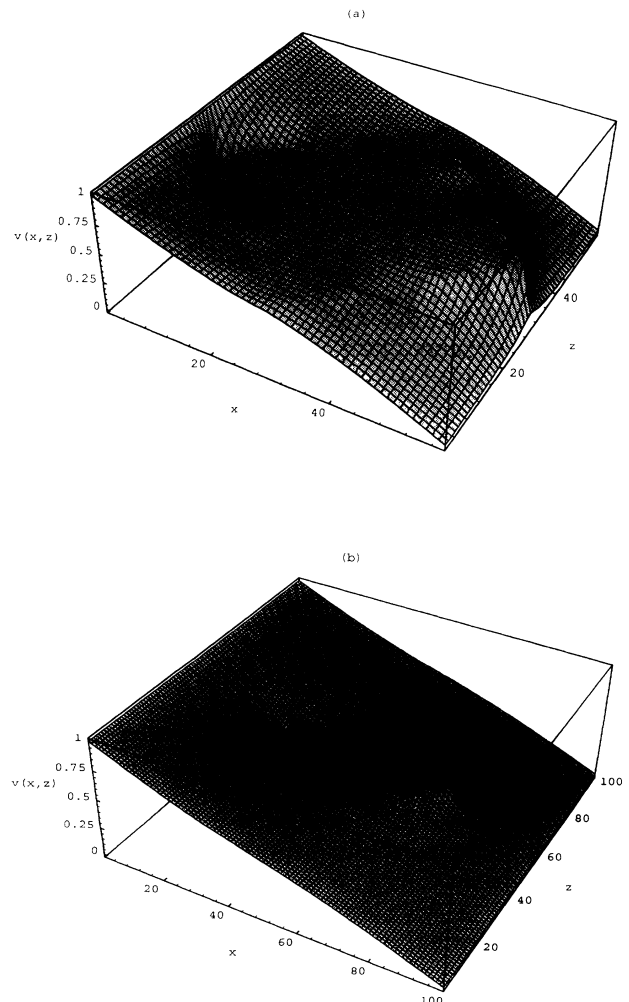


FIG. 3. (a) Electrostatic potential $V(x, z)$ (arbitrary units) for a stage-4 cross fractal (size=54 bonds) embedded in a 58×58 square network with periodic transverse boundary conditions, and subjected to a uniform applied field in the x direction. (b) Same as (a), but for a stage-4 fractal in a 100×100 network.

TABLE III. Same as Table I, but always for a stage-4 fractal and networks of various linear dimension.

Stage	Size	NW size	p_A	$(e_A - 1)/p_A$	$(e_B - 1)/p_A$
4	54	58	0.0743	-12.2	2393
4	54	64	0.061	-15.4	363
4	54	100	0.025	-69.6	70.2

networks there is a smaller (but still very substantial) field enhancement. This is the cause of the large e_i 's in these networks. By contrast, the field is nearly uniform, not only within the highly conducting fractal itself, but also in the nearly enclosed bays outside the fractal. Because of this screening effect, large fractions of the entire network are nearly an equipotential. This effect is, of course, absent in a uniformly random two-dimensional network.

When the fractal forms only a very small volume fraction of the network, the most appropriate measure of nonlinear enhancement is $(e_A - 1)/p_A$ or $(e_B - 1)/p_A$, that is, the *enhancement per unit volume of fractal material*. This quantity is tabulated in the last column of Table III. As the network becomes very large, this quantity should, in principle, saturate at some fixed value $E_k \gg 1$, which increase rapidly with k (although we have not examined fractals and networks large enough to see this saturation). In short, fractal inclusions efficiently increase the nonlinear susceptibilities of their host media and, for a given d_f , become more efficient as they become larger.

In an attempt to understand our numerical results, we compare them to a quasianalytical approximation for χ_e in $d = 2$ and $d = 3$. The approximation is based on a fractal cluster of A particles (cluster dimension R , fractal dimension d_f) embedded in a B host. As discussed in the Appendix, the approximation proceeds in two stages. First, the cluster conductivity and nonlinear susceptibility are calculated in a differential effective-medium scheme. Then the composite susceptibility itself is calculated in the limit of a dilute suspension of clusters.

Figures 4 and 5 show $(e_i - 1)/p_m$ in $d = 2$ and $d = 3$ for a fractal of conductivity σ_m embedded in a host of conductivity σ_i , as calculated using this approximation. p_m represents the composite volume fraction which is made up of material with conductivity σ_m . The horizontal axis denotes the "cluster concentration" $p_{\text{clus}} \equiv (R/a)^{d_f - d}$, where R is the cluster radius measured in units of the smallest particle dimension a , and d_f is the fractal dimension of the cluster. The inset shows the "specific conductivity enhancement" $(\sigma_e - \sigma_i)/(p_m \sigma_i)$ for the same composite, as calculated in the *linear* differential-effective-medium approximation.²⁰

Up to a certain maximum of cluster size, $(e_i - 1)/p_m$ increases greatly. For very large cluster sizes, the specific enhancement begins to decrease and eventually may even become negative, while the enhancement of the *linear* conductivity departs from a power law in p_m . As shown by Ref. 20, such a power law is expected in the limit $\sigma_A/\sigma_B \rightarrow \infty$. Deviations from the power law occur

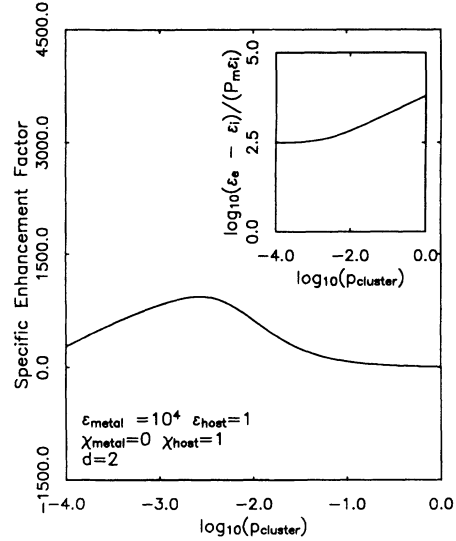


FIG. 4. Specific nonlinear enhancement $(e_i - 1)/p_m$ [Eq. (11)] for a two-dimensional "metal" fractal of dielectric constant $\epsilon_m = 10^4$ embedded in a host of dielectric $\sigma_i = 1$, assuming $\sigma_m = 10000, \sigma_i = 1$. The calculation is carried out using the differential effective-medium approximation [Eqs. (A6) and (A7)] in the high-dilution limit. $(e_i - 1)/p_m$ measures the effective nonlinear enhancement if the host is nonlinear and the inclusion is distributed fractally. The horizontal axis represents the "cluster concentration" $p_{\text{clus}} \equiv (R/a)^{d_f - d}$, where R is the cluster radius measured in units of the smallest particle dimension a ; d is the dimensionality; and d_f is the fractal dimension of the cluster. Inset: specific dielectric enhancement $(\epsilon_e - \epsilon_i)/(p_m \epsilon_i)$ for the same composite, as calculated in the linear differential effective-medium approximation (Ref. 20). ϵ_e is the effective linear dielectric constant of the composite medium containing a dilute suspension of fractals in a host of dielectric constant ϵ_i ; p_m is the total concentration of fractal material in the composite.

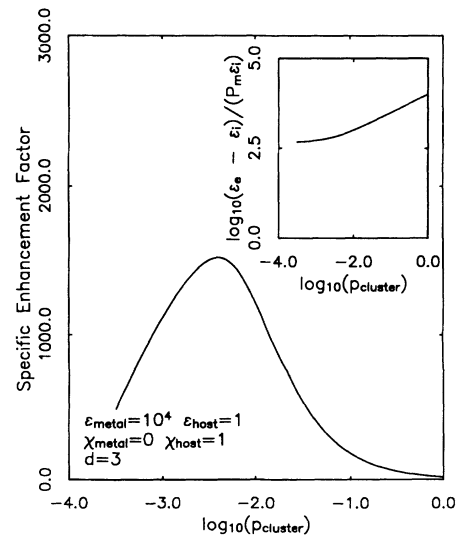


FIG. 5. Same as Fig. 4, but assuming $d = 3$.

when the effective conductivity of the cluster is no longer orders of magnitude larger than that of the host.

The central result of our fractal simulations—that the nonlinear susceptibility of the composite is greatly enhanced by fractal clusters of impurities—is qualitatively consistent with our differential effective-medium approximation. Our numerical cluster sizes are too small, however, to see the predicted saturation in the enhancement.

We note, finally, that the usual decoupling or effective-medium approximation for the nonlinear response of these fractal systems probably fails, because of the large fluctuations of electric field associated with them.²⁸

V. RANDOM MEDIA IN THE THREE DIMENSIONS: NONZERO FREQUENCIES

We turn next to calculations for random media in three dimensions at *finite* frequencies. We describe the insulating bonds by a purely capacitive impedance Z_i ,

$$Z_i = \frac{1}{i\omega C}, \quad (21)$$

and the metallic bond by an RLC circuit. This circuit consists of an inductor \mathcal{L} and a capacitor C' in series, the whole arrangement in parallel with a resistance R which damps the LC resonance. The total impedance of the metallic bond is

$$Z_m = (R + i\omega\mathcal{L}) / (1 + i\omega RC' - \omega^2 LC'). \quad (22)$$

To allow comparison with previous calculations, we assume the same parameters: $C' = C = \mathcal{L} = 1$ and $\tau \equiv \mathcal{L}/R = 10$. As has been discussed previously,²⁹ the

metallic bond is designed to have the impedance of a Drude metal; the LC resonances correspond to the plasmon peaks of such a metal.

Figure 6 plots the real part of the effective network conductivity $\text{Re}\sigma_e(\omega)$ versus concentration p of metal bonds. The calculations are carried out within the EMA (solid curve) and numerically using the transfer-matrix algorithm (circles), as described in Ref. 29. Figs. 7–10 show the effective enhancement factor e_i [cf. Eq. (11)] for metal volume concentrations of 1%, 24.92% (equal to p_c for metallic bonds), 50%, and 90%. In all cases, we have carried out our calculations for $L_x = L_y = 10, L_z = 900$. Evidently, in all cases, there is a large enhancement of the nonlinear susceptibility at appropriate frequencies.

We have attempted to calculate $e_i(\omega)$ and $e_m(\omega)$ for the same model within the EMA. In carrying out the EMA calculations, we use *both* the decoupling approximation, Eq. (12), and the *linear* EMA, Eq. (14). Although the linear version of this EMA describes our linear results well (cf. Fig. 6), this version of the nonlinear EMA misses most of the frequency-dependent structure seen in the numerical e_A and e_B . This is illustrated in Fig. 7, which shows the EMA at a metal concentration of 1%. In this case, the EMA does reproduce the small peak in e_m near $\omega = 0.57\omega_p$, but misses the larger peak at lower frequencies. The agreement at other concentrations is worse.

We believe that the discrepancy seen in Figs. 7–10 comes not from the decoupling approximation (12), but from an inaccurate evaluation of the derivative F_i [Eq. (13)]. χ_e is far more sensitive to details of the composite microstructure than is ϵ_e itself, as already noted by Ref. 12. Hence, even if ϵ_e is accurately given by the EMA, the products $F_i|F_i|$ may not be.

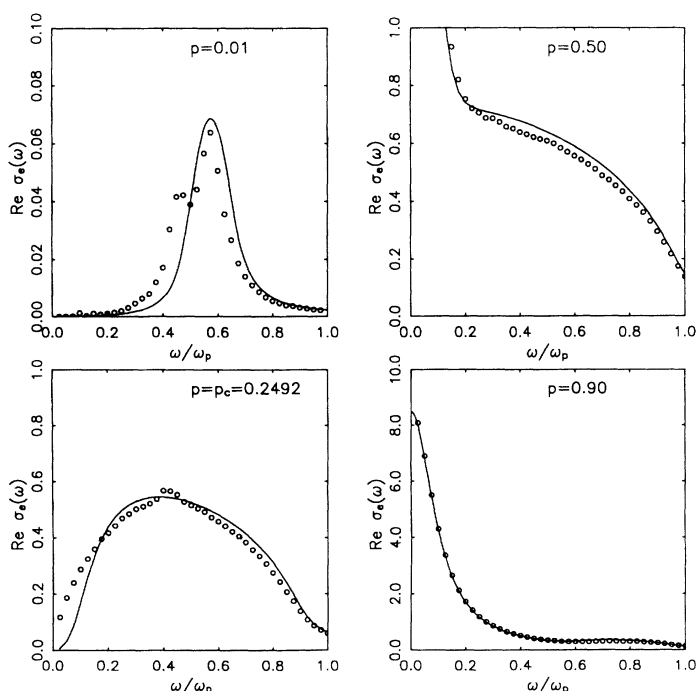


FIG. 6. Real part of the effective conductivity, $\text{Re}\sigma_e(\omega)$, for the three-dimensional composite of Drude metal and insulator described in the text, with $\omega_p\tau = 10$. Solid curves: effective-medium approximation. Circles: numerical simulation using transfer-matrix algorithm. p is the fraction of metal bonds. $p_c = 0.2492$ is the metal percolation threshold.

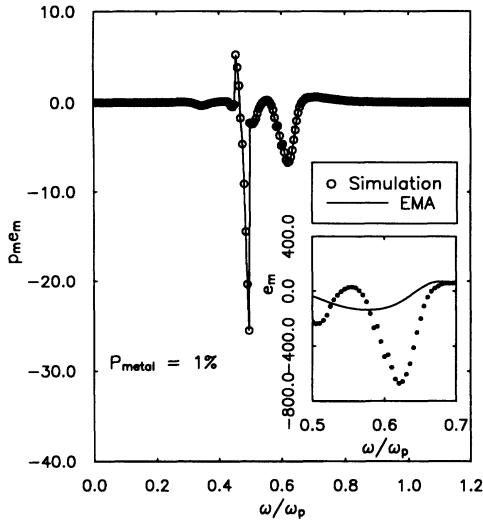


FIG. 7. Metallic nonlinear enhancement factor e_m , for the composite of Fig. 6, plotted as a function of frequency, for metal concentration $p_m=1\%$, as calculated numerically for a $10 \times 10 \times 900$ network. Inset: enlargement of frequency range near $0.57\omega_p$. Dots and circles denote calculated points. The solid line in the main part of the plot merely connects the calculated points, while the solid line in the inset represents the EMA.

To demonstrate this sensitivity, we have calculated ϵ_e at a volume fraction of 90% metal by adding to the EMA results [Eq. (14)] an arbitrary unphysical “correction” $\Delta\epsilon_e(\omega)$ given by

$$\Delta\epsilon_e(\omega) = \epsilon_m \left[1 + \sum_{\lambda} \frac{f_{\lambda} \delta\epsilon(\omega)}{\epsilon_m + g_{\lambda} \delta\epsilon(\omega)} \right], \quad (23)$$

where g_{λ} and f_{λ} are the depolarization factors and weights of some additional hypothetical resonances in the composite beyond those contained in the EMA, and $\delta\epsilon(\omega) = \epsilon_i(\omega) - \epsilon_m(\omega)$. We assume five additional resonances, each with weight $f_{\lambda} = 0.005$, with depolarization factors $g_{\lambda} = 0.2, 0.4, 0.5, 0.7$, and 0.9 . The corresponding derivatives F_i are easily calculated, and both ϵ_e and e_m

evaluated with and without the new resonances. (The results for e_m are shown in Fig. 12 at a concentration of 90% metal.) We have checked that the resonances produce an undetectably small change in ϵ_e , relative to the usual EMA. Nevertheless, these same resonances clearly produce a huge change in e_m , with conspicuous and sharp structure. Even though we have made no effort to fit our results to the numerically calculated ϵ_e and χ_e , it is clear that even tiny deviations from the EMA form for ϵ_e can lead to huge changes in χ_e . We conclude that the decoupling approximation may be accurate, but that even if it is, it must be used with the correct form for the F derivatives, in order to produce the numerically determined χ_e .

Certainly the most striking feature of our finite-frequency results is the remarkable sharp structure in e_i at finite frequencies, in the range $0.3 < \omega/\omega_p < 0.6$ for various metal volume fractions. We do not know the origin of these striking structures, but speculate that they are associated with some (possibly localized) surface-plasmon resonances (*LRC* resonances in the language of our random impedance model), which have only a very weak effect on the linear optical properties, but a much stronger influence on the nonlinear optical properties. For example, as noted above, at a concentration of 1% metal, we see indications of a double peak in the linear optical response (corresponding to two surface plasmon resonances—possibly one arising from impedances parallel to the field and one from impedances perpendicular to the field). The corresponding nonlinear response has two very strong peaks, each of which seems to occur at the frequency of one of the two much weaker linear peaks. We have checked that these same structures are present, at least at 1% concentration, even when the transfer-matrix calculation is carried out with other realizations of the disorder, but at present, we are not able to say anything more precise about the sharp structures at this and other concentrations.

We emphasize that the main features of the structure shown in Figs. 7–10 are *reproducible*. To check this, we have carried out calculations at 1% and 90% filling fraction of metal for several different realizations of the disorder. In both cases, similar sharp peaks appear at the

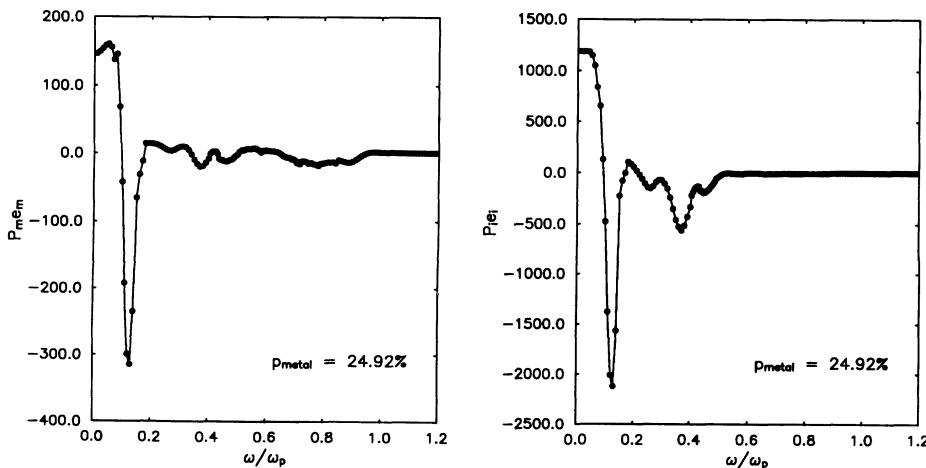


FIG. 8. e_m and insulator enhancement factor e_i for the composite of Fig. 6, for $p_m=24.92\%$, equal to the percolation concentration for metal bonds. $p_i=1-p_m$ is the concentration of insulating bonds. Solid lines simply connect the calculated points.

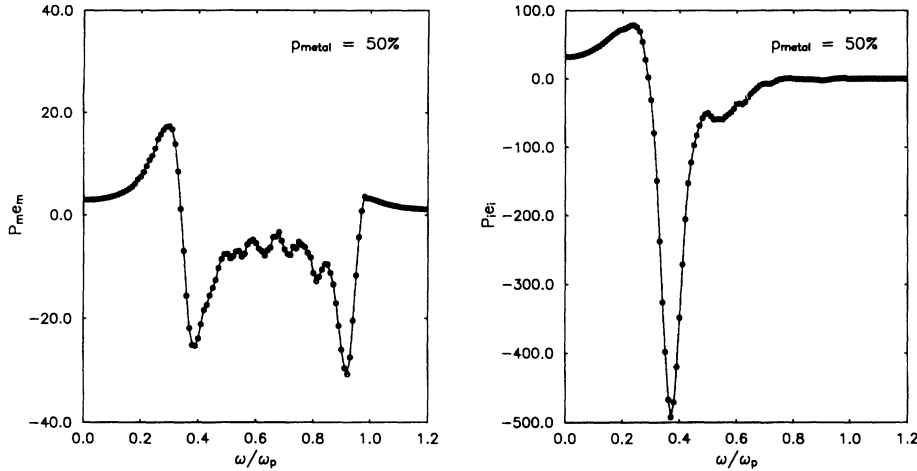


FIG. 9. Same as Fig. 8, but for $p_m = 50\%$.

same frequencies as shown in the figures, although the heights of these peaks does vary from one realization to another.

To summarize this section, we have shown numerically that χ_e for a random metal-insulator composite can be hugely enhanced over that of its constituents. The enhancement is very sensitive to frequency and to composite microstructure. It can possibly be estimated using a simple effective-medium approximation. However, the relevant derivative $F_i \equiv \partial \epsilon_e / \partial \epsilon_i$ is much more difficult to calculate accurately than is ϵ_e itself.

VI. NONLINEAR SUSCEPTIBILITY OF A SUSPENSION OF COATED SPHERES

As a final illustration, we consider χ_e for a dilute suspension of *coated* spheres in a linear host. The spheres have inner radius a , outer radius b ; the core medium, coating, and host have (complex) dielectric constants ϵ_1 , ϵ_2 , and ϵ_3 , respectively. We will calculate the coating enhancement factor e_2 in several limits. Similar calculations have been carried out by Ref. 31, using a rather different formalism.

In the dilute limit, e_2 can be obtained exactly for this composite from Eq. (11). The calculation requires that

the electric field be calculated within the shell in the linear regime. This standard electrostatic calculation is readily accomplished, with the result²²

$$e_2 = \Gamma^3 \Gamma^* \left[\frac{8}{5} \left[\frac{\mu^2 + \mu + 1}{\mu^3} \right] \Lambda^3 \Lambda^* + \frac{2}{5} \frac{\mu + 1}{\mu^2} (3\Lambda^2 \Lambda^* + \Lambda^3) + \frac{18}{5\mu} (\Lambda \Lambda^* + \Lambda^2) + 1 \right], \quad (24)$$

where

$$\Gamma = \frac{3\epsilon_3}{\epsilon_2 + 2\epsilon_3 + 2(\epsilon_2 - \epsilon_3)\Lambda/\mu}, \quad (25)$$

$$\Lambda = \frac{\epsilon_1 - \epsilon_2}{\epsilon_1 + 2\epsilon_2}, \quad (26)$$

$$\mu = \left(\frac{b}{a} \right)^3. \quad (27)$$

Note that Eq. (24) assumes that all shells have the same

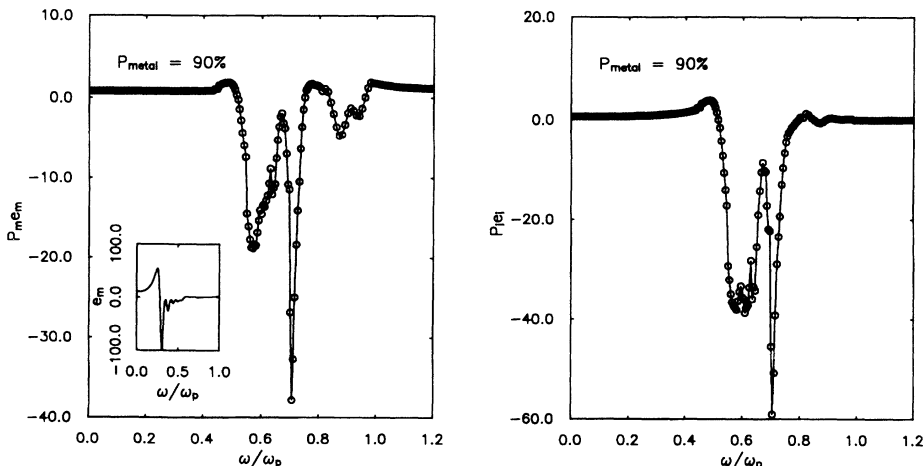


FIG. 10. Same as Fig. 8, but for $p_m = 90\%$. Inset: e_m as calculated in a modified nonlinear effective-medium approximation, as discussed in the text.

ratio b/a , although different particles may have different radii.

We have applied this formula to a composite of small Au particles coated with an assumed nonlinear substance and embedded in a linear host. For the Au dielectric function, we use the approximate analytic fit of Neeves and Birnboim.³¹ For the coating, we assume a constant index of refraction $n_2=1.7$ or $\epsilon_2=2.89$. The host is assumed to have a frequency-independent index of refraction n_3 , but we have considered several values of n_3 and hence $\epsilon_3 \equiv n_3^2$.

If the volume fraction of spheres $p_{\text{sph}} \equiv p_1 + p_2 \ll 1$, the effective linear dielectric constant ϵ_e is accurately calculated in the Maxwell-Garnett approximation (MGA). In this case, the calculation consists of two simple steps. First, one computes the effective dielectric constant of the coated spheres from

$$\epsilon_{\text{sph}} = \epsilon_2 \left[1 + \frac{3p_c \Lambda}{1 - p_c \Lambda} \right], \quad (28)$$

where $p_c = p_1 / (p_1 + p_2)$ is the volume fraction of sphere occupied by the core Au particle. Then ϵ_e is calculated from

$$\epsilon_e = \epsilon_3 \left[1 + \frac{3p_{\text{sph}} t_{\text{sph}}}{1 - p_{\text{sph}} t_{\text{sph}}} \right], \quad (29)$$

where $p_{\text{sph}} = 1 - p_3$ and $t_{\text{part}} = (\epsilon_{\text{sph}} - \epsilon_3) / (\epsilon_{\text{sph}} + 2\epsilon_3)$. Given ϵ_e , χ_e can be calculated using Eqs. (24)–(27) provided that ϵ_3 is replaced by ϵ_e in Eq. (25).

Our results are shown in Figs. 11 and 12, assuming

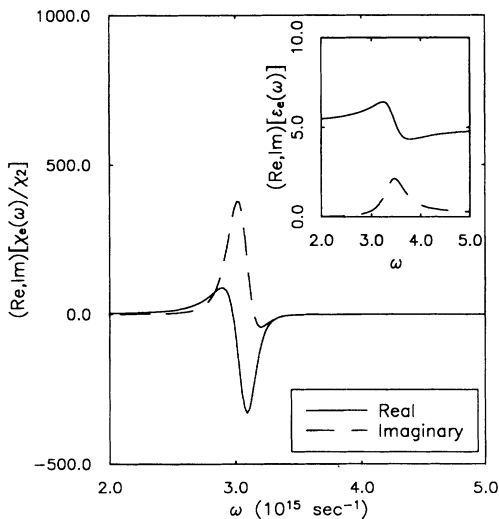


FIG. 11. Nonlinear susceptibility χ_e for a composite consisting of coated spherical Au particles of radius small compared to a wavelength. The coating is assumed to be nonlinear and to have dielectric constant $\epsilon_2=2.89$ independent of frequency and nonlinear susceptibility χ_2 . The dielectric constant of the host is taken as 5.0. The volume ratio of coated sphere to uncoated sphere is 1.25. Plotted are $\text{Re}[\chi_e/\chi_2]$ (solid curve) and $\text{Im}[\chi_e/\chi_2]$ (dashed curve). Inset: $\text{Re}\epsilon_e(\omega)$ and $\text{Im}\epsilon_e(\omega)$ for this composite, as calculated in the Maxwell-Garnett approximation. We always assume a concentration of 3% by volume coated particles.

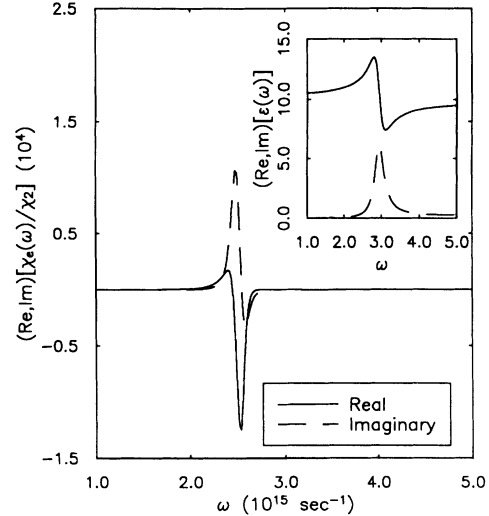


FIG. 12. Same as Fig. 11 but assuming $\epsilon_3=10$.

$p_3=0.03$, and considering two values of ϵ_3 . Evidently, we can obtain very large values of the enhancement factor e_2 (see graphs). The values can be of the order of 10^4 – 10^7 or more. These enhancement factors are almost entirely due to the factor $\Gamma^3\Gamma^*$ in Eq. (24). We have also found that the magnitude of the enhancement factor is remarkably sensitive to the value of ϵ_3 . This is because different values of ϵ_3 have a strong effect on Γ . In general, the larger ϵ_3 , the larger the enhancement factor, and the lower the frequency at which it occurs. We have shown a single example of this effect in the figures.

We have found that the coating thickness also has a significant effect on e_2 , but not so much as the value of ϵ_3 . In general, the thinner the coating, the bigger the enhancement, and the sharper the frequency at which it occurs. On the other hand, the greatest enhancement per coated particle is obtained by making the coating thicker, even at the expense of reducing e_2 . Numerically, there appears to be an optimum coating thickness (defined in this way) which is around 10–20% of the particle radius at $\epsilon_3=5$. In the figures shown, the coating has a volume equal to 25% of the uncoated particle, which is typically near the optimum.

From the figures, it is obviously beneficial under some conditions to make the nonlinear material in the form of a coating on an Au particle, rather than as a homogeneous medium. From Fig. 11, for example, if we use $\mu=1.25$, $\epsilon_3=5$, $\epsilon_2=2.89$, and use for ϵ_1 the dielectric function of Au, then we get a maximum $|e_2|$ of around 4×10^4 . Thus a volume concentration of 3% coated particles still produces $\chi_e/\chi_2 \approx 120$. This enhancement could doubtless be tuned even larger by further manipulation of the parameters ϵ_2 , ϵ_3 , and μ .

VII. DISCUSSION

We have calculated the cubic nonlinear susceptibility of a variety of composite media, modeled as impedance networks in $d=2$ and $d=3$. At zero frequency, we find large enhancements of the susceptibility in random com-

posites, at concentrations near a percolation threshold. We also obtain very large enhancements when one of the components is present in the form of fractal clusters. Both results are in qualitative agreement with predictions based on a simple effective-medium approach. For random binary composites at finite frequencies, we also find huge and highly frequency-dependent enhancements of the nonlinear susceptibility. The relevant frequencies are generally close to the surface-plasmon resonances of the composite, where the electric field is locally much enhanced. In such composites, even though the linear resonance can be calculated in an effective-medium approximation, the nonlinear response is in general much more difficult to predict in this fashion. This is not due to an intrinsic failure of the effective-medium approach itself, but rather because of the great sensitivity of the relevant derivative $F_i = \partial \epsilon_e / \partial \epsilon_i$ to small changes in the local microstructure of the composite.

We have also carried out some simple numerical calculations of the enhancement to be expected when a nonlinear dielectric is coated on a linear core particle and embedded in a host. For Au core particles, we find a huge enhancement near the Au surface plasmon resonance. The low concentration results are in agreement with earlier calculations³¹ based on a slightly different formalism.

On the basis of these calculations, we conclude that binary composites have many ways to produce enormous enhancements in the nonlinear susceptibility. Even at large concentrations, the enhancement is highly frequency-dependent and highly sensitive to composite microstructure. It should therefore be possible to "tune" this enhancement to occur at a desired range of frequencies and hence to produce filters with a range of potential applications.

ACKNOWLEDGMENTS

This work was supported by ARO Grant No. DAAL 03-92-G-0263 and by NSF Grant No. DMR90-20994. Calculations were carried out on the CRAY Y-MP8/8-64 of the Ohio Supercomputer Center with the help of a grant of time. We are grateful for useful conversations with Dr. Van E. Wood, Dr. J. Arthur, and Dr. O. Levy on aspects of this work.

APPENDIX: NONLINEAR DIFFERENTIAL EFFECTIVE-MEDIUM APPROXIMATION

In this appendix, we describe a simple, quasianalytical model for the nonlinear response of fractal clusters in $d=2$ and $d=3$, generalizing a similar scheme developed for linear response by Hui and Stroud.²⁰

As a preliminary, consider a composite containing a small volume concentration p_B of inclusions of type B embedded in a host of type A . The inclusions are assumed to be d -dimensional hyperspheres (i.e., circles or spheres in $d=2$ or 3). The i th component ($i=A$ or B) is assigned conductivity σ_i and nonlinear susceptibility χ_i . The effective conductivity σ_e of the composite can be calculated exactly, to first order to p_B , from the Maxwell-Garnett approximation

$$\sigma_e = \sigma_A (1 + dp_B t_B), \quad (\text{A1})$$

where

$$t_B = \frac{\sigma_B - \sigma_A}{\sigma_B + (d-1)\sigma_A}. \quad (\text{A2})$$

The analogous result for the nonlinear susceptibility χ_e was first obtained by Bergman for the case required here, in which both host and inclusion have a finite susceptibility.¹² It takes the form

$$\chi_e = \chi_A + p_B (\chi_A \lambda_A + \chi_B \lambda_B), \quad (\text{A3})$$

where

$$\begin{aligned} \lambda_A = & \left[-1 + 4t_B + \frac{2(d-1)(d+6)}{d+2} t_B^2 \right. \\ & + \frac{4(d-1)(d-2)}{d+2} t_B^3 \\ & \left. + \frac{d-1}{d+2} \left[d^2 - \frac{7}{3}d + 2 \right] t_B^4 \right] \end{aligned} \quad (\text{A4})$$

and

$$\lambda_B = \left[\frac{d\sigma_A}{\sigma_B + (d-1)\sigma_A} \right]^4. \quad (\text{A5})$$

This result is a generalization of one previously obtained by several authors⁹ for the case where only the inclusion is nonlinear.

We will use this result to obtain an approximate expression for the nonlinear susceptibility of a cluster. The cluster is constructed by starting with a pure A hypersphere. The concentration of B is incrementally increased by adding B material in the form of hyperspheres. Let the cluster at radius R have an effective conductivity $\sigma(R)$ and effective susceptibility $\chi(R)$. Now increase the radius by δR and the volume fraction of type- B material by δp_B . Then from Eqs (A3)–(A5), we immediately obtain

$$d\sigma = \delta p_B [\sigma t_B d] \quad (\text{A6})$$

and

$$d\chi = \delta p_B [\lambda_A \chi + \lambda_B \chi_B], \quad (\text{A7})$$

where t_B , λ_A , and λ_B are given by Eqs. (A2), (A4), and (A5), but with σ_A and χ_A replaced by σ and χ .

Equations (35) and (36) represent ordinary differential equations for the cluster conductivity σ and nonlinear susceptibility χ as functions of p_B . They are readily solved numerically in $d=2$ or $d=3$. The resulting functions $\sigma(p_B)$ and $\chi(p_B)$ represent effective cluster conductivities and susceptibilities for a cluster of concentration p_B . Note that this approach does *not* necessarily assume that the cluster is a fractal. If, however, the cluster is actually a fractal of fractal dimension d_f , then one can relate p_B to the cluster radius R using

$$p_B = 1 - \left(\frac{R}{a} \right)^{(d_f - d)}, \quad (\text{A8})$$

where we are assuming that component A , present in concentration $1 - p_B$, is distributed fractally, and that a is

the linear dimension of the smallest A particle.

Once the cluster parameters σ and χ have been calculated, it remains to calculate σ_e and χ_e for the composite itself. In the dilute limit (volume concentration of clusters much less than unity), these may be obtained simply by another application of Eqs. (A1)–(A5).

¹For a recent review of both electrical and optical properties, see, e.g., D. J. Bergman and D. Stroud, in *Solid State Physics*, edited by H. Ehrenreich and D. Turnbull (Academic, New York, 1992), Vol. 46, pp. 178–320.

²For a recent review emphasizing optical properties, see J. Clerc, G. Giraud, M. Laugier, and J. M. Luck, *Adv. Phys.* **39**, 191 (1990).

³For a recent review, see, e.g., Ref. 1 or B. K. Chakrabarti, *Rev. Solid State Sci.* **2**, 559 (1988).

⁴R. Rammal, C. Tannous, and A.-M. S. Tremblay, *Phys. Rev. A* **31**, 2662 (1985).

⁵R. Rammal, P. Breton, and A.-M. S. Tremblay, *Phys. Rev. Lett.* **54**, 1718 (1985).

⁶L. de Arcangelis, S. Redner, and A. Coniglio, *Phys. Rev. B* **31**, 4725 (1985); **34**, 4656 (1986).

⁷M. A. Dubson, Y. C. Hui, M. B. Weissmann, and J. C. Garland, *Phys. Rev. B* **39**, 6807 (1989).

⁸S. W. Kenkel and J. P. Straley, *Phys. Rev. B* **29**, 6299 (1984).

⁹D. Stroud and P. M. Hui, *Phys. Rev. B* **37**, 8719 (1988).

¹⁰X. C. Zeng, D. J. Bergman, P. M. Hui, and D. Stroud, *Phys. Rev. B* **38**, 10970 (1988); X. C. Zeng, P. M. Hui, D. J. Bergman, and D. Stroud, *Physica A* **157**, 192 (1989).

¹¹R. Blumenfeld and D. J. Bergman, *Phys. Rev. B* **40**, 1987 (1989).

¹²D. J. Bergman, *Phys. Rev. B* **39**, 4598 (1989).

¹³D. C. Wright, Y. Kantor, and D. J. Bergman, *Phys. Rev. B* **33**, 396 (1986).

¹⁴For recent reviews, see, e.g., the articles in *J. Opt. Soc. Am. B* **6** (1989) or C. Flytzanis, *Prog. Opt.* **29**, 2539 (1992).

¹⁵R. Jain and R. C. Lind, *J. Opt. Soc. Am.* **73**, 647 (1983).

¹⁶D. Ricard, P. Roussignol, and C. Flytzanis, *Opt. Lett.* **10**, 511 (1985); F. Hache, D. Ricard, and C. Flytzanis, *J. Opt. Soc. Am. B* **3**, 1647 (1986); F. Hache, D. Ricard, C. Flytzanis, and U. Kreibig, *Appl. Phys. A* **47**, 347 (1988).

¹⁷P. Roussignol, D. Ricard, J. Lukasik, and C. Flytzanis, *J. Opt. Soc. Am. B* **4**, 5 (1987).

¹⁸See, for example, D. Stroud and Van E. Wood, *J. Opt. Soc. Am. B* **6**, 778 (1989); A. E. Neeves and M. H. Birnboim, *ibid.* **6**, 787 (1989); Y. Q. Li, C. C. Sung, R. Inguva, and C. M. Bowden, *ibid.* **6**, 814 (1989).

¹⁹J. W. Haus, N. Kalyaniwalla, R. Inguva, M. Bloemer, and C. M. Bowden, *J. Opt. Soc. Am. B* **6**, 797 (1989); J. W. Haus, R. Inguva, and C. M. Bowden, *Phys. Rev. A* **40**, 5729 (1990); M. J. Bleomer, P. R. Ashley, J. W. Haus, N. Kalyaniwalla, and C. R. Christensen, *IEEE J. Quantum Electron.* **QE-26**, 1075 (1990).

²⁰P. M. Hui and D. Stroud, *Phys. Rev. B* **33**, 2163 (1986).

²¹N. Kalyaniwalla, J. W. Haus, R. Inguva, and M. H. Birnboim, *Phys. Rev. A* **42**, 5613 (1990).

²²K. W. Yu, P. M. Hui, and D. Stroud, *Phys. Rev. B* **47**, 14 150 (1993).

²³A. Aharony, *Phys. Rev. Lett.* **58**, 2726 (1987).

²⁴B. Derrida and J. Vannimenus, *J. Phys. A* **15**, 557 (1982).

²⁵E. Duering, M. Murat, A. Aharony, and D. J. Bergman (unpublished).

²⁶C. S. Yang and P. M. Hui, *Phys. Rev. B* **44**, 12 559 (1991).

²⁷I. H. Hoffmann and D. Stroud, *Phys. Rev. B* **43**, 9965 (1991).

²⁸V. Shalaev and co-workers have carried out extensive calculations of the nonlinear response of fractals in the optical regime, using methods different from those described here. See A. V. Butenko, V. M. Shalaev, and M. I. Stockman, *Zh. Eksp. Teor. Fiz. [Sov. Phys. JETP]* **67**, 60 (1988); *Z. Phys. D* **10**, 81 (1988); S. G. Rautian, V. P. Safonov, P. A. Chubakov, V. M. Shalaev, and M. I. Stockman, *Pis'ma Zh. Eksp. Teor. Fiz.* **47**, 200 (1988) [*JETP Lett.* **47**, 243 (1988)]; V. M. Shalaev, M. I. Stockman, and R. Botet, *Physica A* **185**, 181 (1992).

²⁹X. Zhang and D. Stroud, *Phys. Rev. B* **48**, 6658 (1993).

³⁰X. Zhang (unpublished).

³¹A. E. Neeves and M. H. Birnboim, *J. Opt. Soc. Am. B* **6**, 787 (1989). We use their Eq. (13). Note that the plus sign in the denominator of the third term should be a negative sign.

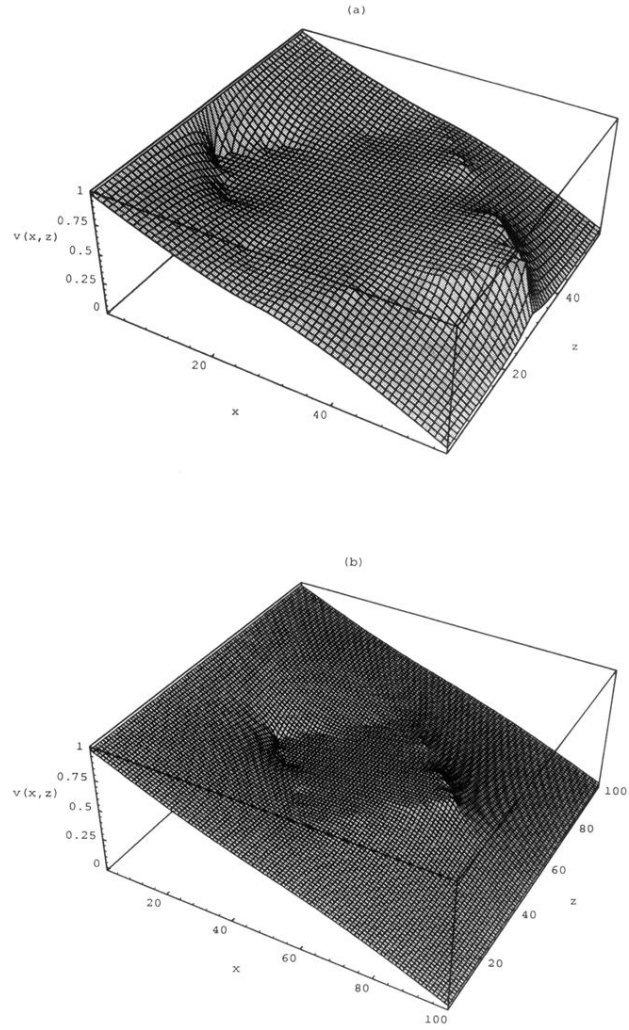


FIG. 3. (a) Electrostatic potential $V(x, z)$ (arbitrary units) for a stage-4 cross fractal (size=54 bonds) embedded in a 58×58 square network with periodic transverse boundary conditions, and subjected to a uniform applied field in the x direction). (b) Same as (a), but for a stage-4 fractal in a 100×100 network.